Comparative Biochemistry and Physiology - Part D: Genomics and Proteomics 59 (2026) 101798

Contents lists available at ScienceDirect

Comparative Biochemistry and Physiology - Part D: Genomics and Proteomics

journal homepage: www.elsevier.com/locate/cbpd

Research article

High-dose ginsenoside Rg5 induces tissue-specific metabolic and transcriptional responses in muscle and liver of grass carp (*Ctenopharyngodon idella*)

Li Ren [a,b,c,*,1], Xiaohuan Han [a,1], Qingxi Wang [d,1], Kai Yang [a], Jinhui Zhang [a], Ruyi Zhang [a], Yude Wang [a,b,c], Yiyan Zeng [a], Ling Liu [a], Wei Liu [a], Wuhui Li [a,b,c,*], Shaojun Liu [a,b,c,*]

[a] *Engineering Research Center of Polyploid Fish Reproduction and Breeding of the State Education Ministry, College of Life Sciences, Hunan Normal University, Changsha, 410081, Hunan, China*
[b] *Yuelushan Laboratory, Changsha, 410128, Hunan, China*
[c] *Hunan Yuelu Mountain Science and Technology Co., Ltd. for Aquatic Breeding, Changsha, 410081, Hunan, China*
[d] *Hunan Traditional Chinese Medical College, Changsha, 410081, Hunan, China*

ARTICLE INFO

Edited by Chris Martyniuk

Keywords:
Ctenopharyngodon idella
Ginsenoside Rg5
Growth-stress trade-off
Somatic growth
Multi-omics

ABSTRACT

Optimizing growth efficiency in grass carp (*Ctenopharyngodon idella*) is a key objective in aquaculture, yet the broader physiological responses to intensive growth-promoting treatments remain incompletely characterized. In this study, whole-genome resequencing, transcriptomics, and targeted metabolomics were integrated to assess tissue-specific responses to high-dose ginsenoside Rg5 administration. Whole-genome resequencing suggested highly comparable genetic backgrounds among experimental groups. High-dose Rg5 treatment was associated with marked myofiber hypertrophy and increased expression of *igf1r* and muscle structural genes, while hepatic *igf1* expression was reduced. In muscle tissue, nicotinamide abundance increased by 20.8-fold, accompanied by elevated *nampt* expression. In the liver, 3-hydroxypropionic acid (3-HP) levels were strongly reduced, together with increased expression of gluconeogenic enzymes (*g6pc* and *pc*). In addition, expression of the endoplasmic reticulum stress marker *hspa5* was substantially elevated, and transcripts of circadian regulators (*clock* and *arntl*) were reduced across tissues. These observations indicate that high-dose Rg5–induced growth is accompanied by coordinated metabolic and transcriptional adjustments in muscle and liver, highlighting potential physiological considerations associated with pharmacological growth enhancement.

1. Introduction

Grass carp (*Ctenopharyngodon idella*) is a major species in global freshwater aquaculture and contributes substantially to animal protein production (Hu et al., 2021; Wang et al., 2024). To improve production efficiency, increasing attention has been directed toward natural growth-promoting compounds as alternatives to traditional agents associated with environmental concerns (Chakraborty et al., 2014). Ginsenosides, a group of bioactive triterpene saponins derived from *Panax ginseng*, have been widely reported to modulate energy metabolism, inflammatory responses, and circadian-related gene expression in vertebrates (Zhang et al., 2024).

Ginsenoside Rg5 is particularly notable. In mammalian models, Rg5 acts as an insulin-like growth factor 1 receptor (Igf1r) agonist, promoting angiogenesis (Cho et al., 2015). Furthermore, recent evidence indicates that it can actively promote myogenesis and prevent skeletal muscle atrophy via the p38MAPK and Akt/mTOR signaling pathways (Kim et al., 2023). However, somatic growth in vertebrates involves coordinated regulation across multiple tissues, particularly the liver and skeletal muscle, which together integrate endocrine, metabolic, and energetic signals (Chakravarthy et al., 2020). Direct pharmacological stimulation of peripheral growth pathways may therefore alter the

* Corresponding authors at: Engineering Research Center of Polyploid Fish Reproduction and Breeding of the State Education Ministry, College of Life Sciences, Hunan Normal University, Changsha, 410081, Hunan, China.
E-mail addresses: rl@hunnu.edu.cn (L. Ren), 202101055@hunnu.edu.cn (W. Li), lsj@hunnu.edu.cn (S. Liu).
[1] These authors contributed equally to this work.

https://doi.org/10.1016/j.cbd.2026.101798
Received 3 February 2026; Received in revised form 26 February 2026; Accepted 27 February 2026
Available online 3 March 2026
1744-117X/© 2026 Elsevier Inc. All rights are reserved, including those for text and data mining, AI training, and similar technologies.

balance of this coordination, especially under high-dose exposure.

Growth-related physiological responses are commonly constrained by trade-offs in energy allocation between anabolic processes and stress-related maintenance (Karasov et al., 2017; Kim et al., 2024). While moderate ginseng supplementation has been associated with improved metabolic and circadian-related outcomes (Zhang et al., 2024), the systemic consequences of high-dose pharmacological stimulation remain insufficiently characterized. In particular, sustained activation of peripheral growth pathways may be accompanied by altered hepatic metabolism and stress responses, with potential secondary effects on circadian gene expression (Gao et al., 2019; Dijk and Duffy, 2020).

In this study, we applied an integrated multi-omics strategy combining whole-genome resequencing (WGS), transcriptomics, and targeted metabolomics to investigate tissue-specific responses to high-dose Rg5 in grass carp. By first excluding genetic background variation, we focused on physiological and molecular changes associated with Rg5 treatment. Our results reveal coordinated alterations in muscle growth, hepatic metabolism, and stress-related pathways, providing insights into systemic responses accompanying pharmacologically enhanced growth.

2. Materials and methods

2.1. Experimental animals and maintenance

All experimental procedures involving animals were reviewed and approved by the Animal Ethics Committee of Hunan Normal University, Hunan, China. Grass carp (*Ctenopharyngodon idella*) fingerlings (5 months old) were obtained from a commercial hatchery in Changsha, Hunan Province, China (112.64° E, 28.32° N). Before the experiment, uniformly sized and healthy individuals (initial mean weight: 65.6 ± 15.2 g) were selected and acclimated for 7 days in a recirculating aquaculture system. The formal experimental period spanned 35 days, from September 12 to October 16, 2024. During this period, water temperature was monitored twice daily (09:30 and 17:30) and fluctuated naturally between 22.2 °C and 33.3 °C due to the seasonal transition. Fish were fed commercial pellets (Tongwei Co., Ltd., China) twice daily to apparent satiation. To ensure optimal water quality, uneaten feed was siphoned out 20 min post-feeding. Continuous aeration was provided to maintain dissolved oxygen levels above 6.0 mg/L, while ammonia-nitrogen levels were maintained below 0.05 mg/L.

2.2. Drug preparation and experimental design

Ginsenoside Rg5 (purity >98%, Cat. No. HY-N0908) was purchased from MedChemExpress (USA). Due to the hydrophobic nature of the compound, a specialized solubilization protocol was used to ensure bioavailability. Briefly, 9.3 mg of Rg5 powder was dissolved in 0.1 mL of fresh DMSO (which has been shown to be non-toxic at the administered volume) with sonication at 37 °C for 15 min. This concentrated solution was then slowly diluted with 0.9 mL of 20% sulfobutyl ether-β-cyclodextrin (SBE-β-CD, Sigma-Aldrich, USA) in saline to obtain a clear, stable stock solution at a concentration of 9.3 mg/mL. The final vehicle composition was 10% DMSO and 90% (20% SBE-β-CD in saline).

A total of 24 fish were randomly assigned to four groups (initial $n = 6$ per group): a solvent control group and three experimental groups receiving increasing doses of Rg5. The experimental groups received single intraperitoneal injections of Rg5 solutions at concentrations of 0.58 mg/mL (group 1, low dose), 2.325 mg/ mL (group 2, medium dose), and 9.3 mg/ mL (group 3, high dose), corresponding to approximate dosages of 0.29, 1.16, and 4.65 mg/kg body weight, respectively (injection volume: 0.05 mL/fish). The control group received an equivalent volume of the vehicle solvent. During the experimental period, mortality resulted in a final sample size of $n = 5$ for the control group, n = 5 for group 1, n = 5 for group 2, and $n = 6$ for group 3 (Table S1).

At the conclusion of the 35-day experiment, all individuals were weighed, and the weight gain rate (WGR) was calculated. Based on the comprehensive evaluation of growth performance across the dosage gradient, the high-dose group exhibited the most pronounced and consistent phenotypic divergence from the control group. Therefore, all surviving individuals from the control group (n = 5) and the high-dose group (n = 6) were selected as representative cohorts for subsequent transcriptomic, metabolomic, and genomic analyses to maximize the detection of treatment-associated molecular signatures. To ensure maximum data integration and eliminate inter-individual variability, the exact same set of 11 fish was used for all downstream analyses: whole-genome resequencing (WGS), transcriptomics, targeted metabolomics, and histological examination. Individual growth data and their specific allocation for each analysis are detailed in Table S1.

2.3. Sample collection and histological analysis

To eliminate the potential interference of chemical anesthetics on the transcriptomic and metabolomic profiles, fish were euthanized by immediate spinal cord transection. For histological examination, dorsal white muscle blocks (approximately 1.0 cm × 1.0 cm × 0.5 cm) were excised and immediately fixed in Bouin's solution for 24 h. The fixed tissues were subsequently transferred to 70% ethanol, dehydrated through a graded ethanol series, cleared in xylene, and embedded in paraffin wax. Continuous sections with a thickness of 5 μm were prepared using a rotary microtome (Leica RM2235, Germany) and stained with hematoxylin and eosin following standard protocols. Morphological images were captured using an optical microscope (Olympus BX53, Japan) at 200× and 400× magnification. Muscle fiber cross-sectional area and equivalent diameter were quantified using ImageJ software (NIH, USA). Specifically, for each individual fish ($n = 5$ or 6), non-overlapping histological images were captured. From these images, a minimum of 100 intact muscle fibers per individual were randomly selected and measured to calculate the mean cross-sectional area and equivalent diameter.

2.4. Targeted metabolomics analysis

To comprehensively profile the metabolic alterations, a broad-spectrum targeted metabolomics approach was employed to quantify 488 functional metabolites, covering amino acids, organic acids, nucleotides, carbohydrates, and fatty acids. Frozen tissue samples (25 mg) were weighed into 2.0 mL tubes. Metabolite extraction was performed by adding 500 μL of pre-cooled extraction buffer (methanol:water = 4:1, *v*/v) containing a mixture of isotope-labeled internal standards, along with two 3.2 mm steel beads. Samples were homogenized at 40 Hz for 4 min using a high-throughput tissue grinder (JXFSTPRP-24, Shanghai, China), followed by sonication in an ice-water bath for 5 min. This homogenization and sonication cycle was repeated three times. Samples were then incubated at −40 °C for 1 h to precipitate proteins, followed by centrifugation at 12,000 rpm (13,800 ×g) and 4 °C for 15 min. The supernatant was collected for LC-MS/MS analysis. Quality control samples were prepared by pooling equal aliquots of the supernatants from all samples to monitor system stability and data reproducibility throughout the analysis.

Chromatographic separation was performed using an Agilent 1290 Infinity II UHPLC system (Agilent Technologies, USA). To ensure broad coverage of metabolites with diverse polarities, two chromatographic methods were applied. For the Reversed-Phase system, an ACQUITY UPLC BEH C18 column (1.7 μm, 2.1 mm × 150 mm, Waters) was employed with Mobile Phase A (water with 0.1% formic acid) and Mobile Phase B (methanol:water, 95:5, containing 10 mmol/L ammonium formate). For the Hydrophilic Interaction Liquid Chromatography system, an Atlantis Premier BEH *Z*-HILIC column (1.7 μm, 2.1 mm × 150 mm, Waters) was used with Mobile Phase A (water:acetonitrile, 10:90, with 10 mmol/L ammonium acetate) and Mobile Phase B (water:

acetonitrile, 90:10, with 10 mmol/L ammonium acetate). The injection volume was 1 μL, and the auto-sampler was maintained at 6 °C.

Mass spectrometric detection was carried out on a SCIEX Triple Quad 6500+ mass spectrometer (AB Sciex, USA) equipped with an electrospray ionization source operating in multiple reaction monitoring (MRM) mode. Key source parameters included: Curtain Gas at 35 psi, IonSpray Voltage at +5000 V (positive mode) or − 4500 V (negative mode), Source Temperature at 400 °C, and Ion Source Gases 1 and 2 at 50 psi. Raw data were acquired and processed using SCIEX Analyst Workstation software (v1.7.3) and BIOTREE BioBud (v2.0.4). Compound identification was confirmed by comparing retention times and MRM transitions with an in-house standard library. Absolute metabolite concentrations (nmol/g) were calculated based on calibration curves constructed using authentic standards.

2.5. Nucleic acid extraction, library preparation, and sequencing

Genomic DNA was extracted from muscle tissue using the DNeasy Blood & Tissue Kit (Qiagen, Germany), while total RNA was extracted from liver and muscle tissues using TRIzol reagent (Invitrogen, USA). Nucleic acid concentration and purity were verified using a NanoDrop One spectrophotometer (Thermo Fisher Scientific, Waltham, MA, USA) ensuring OD260/280 > 1.8, and RNA integrity was assessed using an Agilent 2100 Bioanalyzer (Agilent Technologies, USA) with an RNA integrity number > 7.0. For whole genome resequencing, 1 μg of genomic DNA was fragmented using a covaris system. The fragments underwent end-repair, A-tailing, and adapter ligation. The resulting products were heat-denatured and circularized to form single-stranded circular DNA, which was subsequently amplified into DNA Nanoballs (DNBs) via rolling circle replication (RCR). Sequencing was performed on the DNBSEQ-T7 platform (MGI Tech, Shenzhen, China) using a paired-end 150 bp (PE150) strategy. For RNA-Seq, mRNA was enriched using oligo (dT) magnetic beads, fragmented, and reverse-transcribed to cDNA. Sequencing libraries were constructed following the standard DNBSEQ protocol and sequenced on the DNBSEQ-T7 platform (PE150).

2.6. Bioinformatics and statistical analysis

All bioinformatics analyses were based on the high-quality T2T reference genome (NCBI accession number: GCA_049919795.1). Raw reads were processed using fastp (v0.23.2) to remove adapters and low-quality bases (Chen et al., 2018). For genomic analysis, clean reads were aligned to the reference genome using BWA-MEM (v0.7.17) (Li and Durbin, 2010). Read sorting and PCR duplicate marking were performed using Samtools (v1.13) (Li et al., 2009) and Picard (v3.0.0, https://broadinstitute.github.io/picard/), respectively. Variant calling followed the GATK4 (v4.6.2.0) pipeline (Mckenna et al., 2010), utilizing HaplotypeCaller for GVCF generation and GenotypeGVCFs for joint genotyping. High-confidence variants were obtained by applying hard filtering criteria: QD < 2.0, MQ < 40.0, FS > 60.0, SOR > 3.0, MQRankSum < −12.5, and ReadPosRankSum < −8.0. Population differentiation index (Fst) and nucleotide diversity (π) were calculated using VCFtools with a 10 kb sliding window (step size 2 kb) (Danecek et al., 2011). Functional annotation of variants was performed using SnpEff (v5.0) (Cingolani et al., 2012) with a custom database constructed from the reference genome and GFF annotation files. For transcriptomic analysis, clean reads were mapped using HISAT2 (v2.2.1) (Kim et al., 2019) with the –dta parameter, and gene counts were quantified using featureCounts (v2.1.1) (Liao et al., 2014). Expression levels were normalized to transcripts per million (TPM). Gene expression levels for key candidates were visualized based on Normalized Transcripts per Million (TPM) values derived from the RNA-Seq dataset. Differential expression analysis was conducted using the R package DESeq2 (Love et al., 2014), with significance thresholds set at $|\log_2 \text{FoldChange}| > 1$ and $p < 0.05$. Functional enrichment analyses (GO and KEGG) were performed using the clusterProfiler package (Yu et al., 2012). To elucidate gene-metabolite regulatory networks, transcriptomic and metabolomic datasets were integrated using O2PLS modeling (OmicsPLS package) (Bouhaddani et al., 2018) and Pearson correlation analysis. All statistical visualizations were generated in the R environment (v4.4.1) using ggplot2 and pheatmap packages.

3. Results

3.1. Ginsenoside Rg5 induces somatic growth via muscle hypertrophy

To systematically evaluate the growth-promoting potential of Rg5, we conducted a 35-day gradient dosage experiment. Continuous monitoring indicated that water temperature fluctuated naturally within a physiological range (22.2 °C - 33.3 °C) without pronounced environmental shock (Fig. 1A), effectively ruling out environmental stress as a confounding factor. Growth performance assessment revealed a dose-dependent promoting trend. The high-dose group exhibited the most prominent growth advantage, with an average weight gain rate (WGR) of 16.35%, which was higher than that of the control group (12.86%, Fig. 1B, Table S1).

To elucidate the cellular basis of this weight gain, we performed histological analysis on dorsal white muscle tissues. H&E staining showed marked expansion of muscle fibers in the Rg5-treated individuals compared to the control (Fig. 1C). Quantitative morphometric analysis confirmed significant hypertrophy: the muscle fibers of the high-dose group demonstrated a statistically significant increase in both cross-sectional area and equivalent diameter compared to control ($p < 0.05$, Fig. 1D). Thus, the increased muscle mass in the high-dose group was accompanied by a significant increase in fiber size.

3.2. Whole-genome resequencing reveals a highly consistent genetic background across groups

To exclude the potential confounding effects of genetic heterogeneity on the observed growth phenotypes, we performed whole-genome resequencing. A total of 11 individuals from the control and high-dose groups were sequenced, generating 132.28 Gb of raw data (Table S2). Alignment to the high-quality T2T reference genome of grass carp yielded an average mapping rate of 99.68%, which served as the basis for subsequent SNP analysis (Table S3). Principal component analysis (PCA) revealed extensive overlap between individuals from the control and high-dose groups in the genetic space, with no distinct subpopulation separation (Fig. 2A), indicating a consistent genetic background between the two groups.

A genome-wide scan for selection signals was performed using the fixation index (Fst). Although the genome-wide average weighted Fst was extremely low (≈ 0.00007), sporadic loci with high differentiation (Fst ≈ 1.0) were observed across the genome (Fig. 2B), potentially attributable to the small sample size effect ($n = 5$ vs. $n = 6$) and random genetic drift. To determine whether these variants drove the growth phenotype, we performed precise association mapping between these regions and gene functions. The results showed that core genes governing the GH-IGF growth axis (e.g., *igf1*), lipid synthesis (*srebp*), and key metabolism genes (e.g., *cyp450* family) were all located in regions of negligible differentiation (Fst ≈ 0) (Fig. 2B, red labeled points). This suggests that, despite random background genomic noise, the two experimental groups are genetically highly conserved in functional core pathways. These data show that the core metabolic and growth-related loci reside in genomic regions with low differentiation between the experimental groups.

3.3. Landscape of tissue-specific transcriptional and metabolomic reprogramming

To investigate the systemic molecular mechanisms underlying Rg5-induced growth, we integrated transcriptomic and targeted

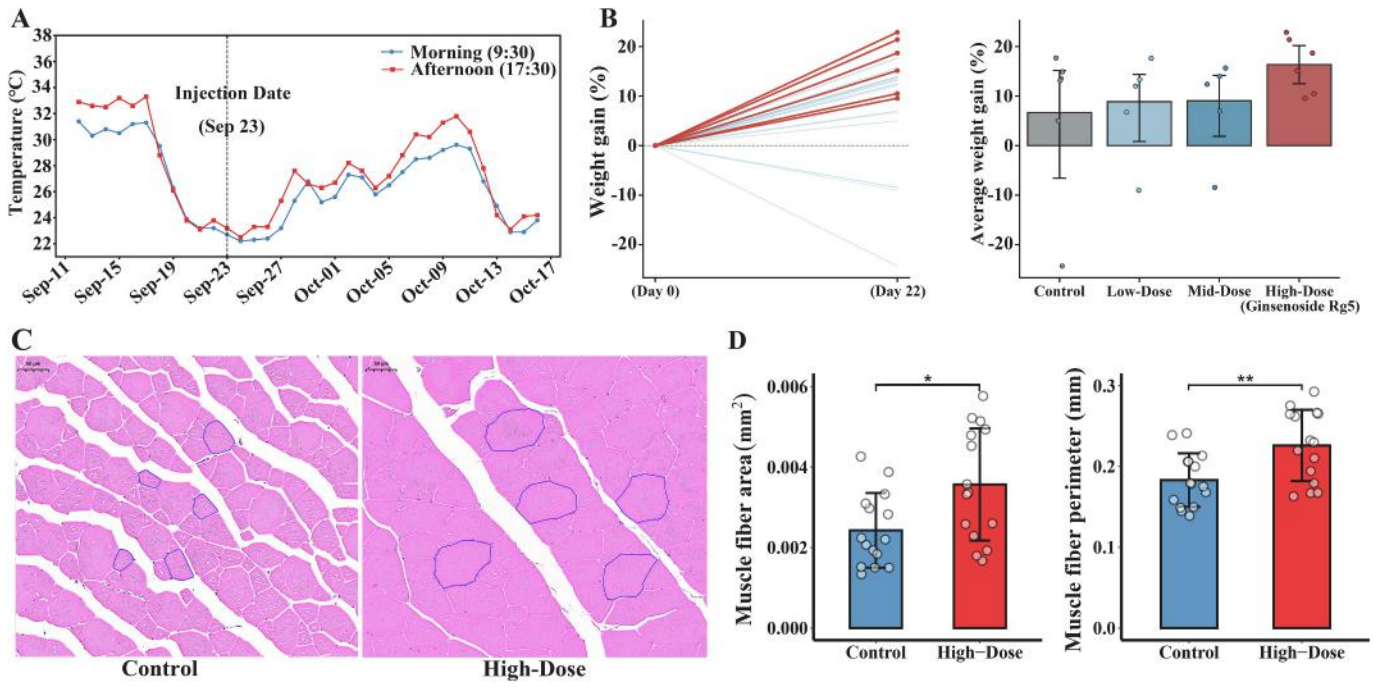


Fig. 1. Experimental design and phenotypic characterization of *Ctenopharyngodon idella* under Rg5 treatment.
(A) Daily water temperature profile during the 35-day experimental period. (B) Comparison of weight gain rate between the control group ($n = 5$) and high-dose group ($n = 6$). (C) Representative H&*E*-stained transverse sections of dorsal white muscle tissue. Scale bar = 50 μm. (D) Morphometric quantification of muscle fibers (control, n = 5; high-dose, n = 6). Data are presented as mean ± SEM. $p < 0.05$ (*t*-test).

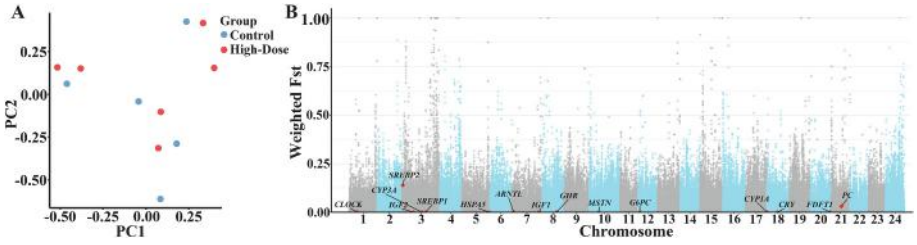


Fig. 2. Genomic background assessment via whole-genome resequencing.
(A) Principal Component Analysis (PCA) of genomic variants (SNPs) for all 11 individuals. (B) Genome-wide manhattan plot of the fixation index (Fst) calculated in 10 kb sliding windows. Red diamonds indicate the genomic positions of core genes involved in growth (*igf1* and *ghr*), lipid metabolism (*srebp*), and drug metabolism (*cyp* family), showing negligible differentiation (Table S6). (For interpretation of the references to colour in this figure legend, the reader is referred to the web version of this article.)

metabolomic profiling of liver and muscle tissues. Consistent with the phenotypic evaluation, transcriptomic and metabolomic analyses were focused on the control and high-dose groups, which represented the extremes of the growth response. A cumulative total of 168.59 Gb of high-quality data was obtained, with an average mapping rate of 95.13% to the reference genome (Tables S4-S5). Transcriptomic landscapes revealed a profound and coordinated response to high-dose Rg5 treatment (Fig. 3A). PCA plots showed a clear separation between experimental groups along the first principal component (PC1), which accounted for an notable 58% of the total variance in the muscle—significantly higher than the 31% observed in the liver—indicating that skeletal muscle exhibits a pronounced transcriptional response to Rg5 treatment. Differential expression analysis (Fig. 3B) identified 1700 differentially expressed genes (DEGs) in the liver and 1950 DEGs in the muscle.

To validate the metabolic consequences of these transcriptional shifts, we performed targeted metabolomics on the same tissues. A total of 488 metabolites were detected, with 337 identified in the liver and 278 in the muscle. PCA of the metabolomic profiles showed distinct clustering between groups in both tissues (Fig. 3C). While metabolic divergence was clear, it appeared more conservative than the transcriptomic response. Differential analysis ($p < 0.05$) revealed 40 significant differential metabolites in the liver and 47 in the muscle (Fig. S3). Overall, the high degree of concordance between the two omics layers indicates coordinated transcriptional and metabolic changes across tissues following Rg5 treatment.

3.4. Local growth-associated signaling and metabolic features in skeletal muscle

Following the observation that high-dose Rg5 significantly induces muscle hypertrophy in grass carp (Fig. 1), we investigated the underlying molecular regulatory mechanisms. While conventional paradigms posit that muscle growth is primarily governed by hepatic endogenous *igf1*, our data revealed a paradoxical downregulation of hepatic *igf1* expression following Rg5 treatment (Table S6). This pattern suggests that muscle growth may proceed through enhanced local receptor-level signaling that is less dependent on hepatic *igf1* expression. Transcriptomic profiling identified a significant upregulation of the local insulin-like growth factor 1 receptor (*igf1r*) in skeletal muscle (Fig. 4A

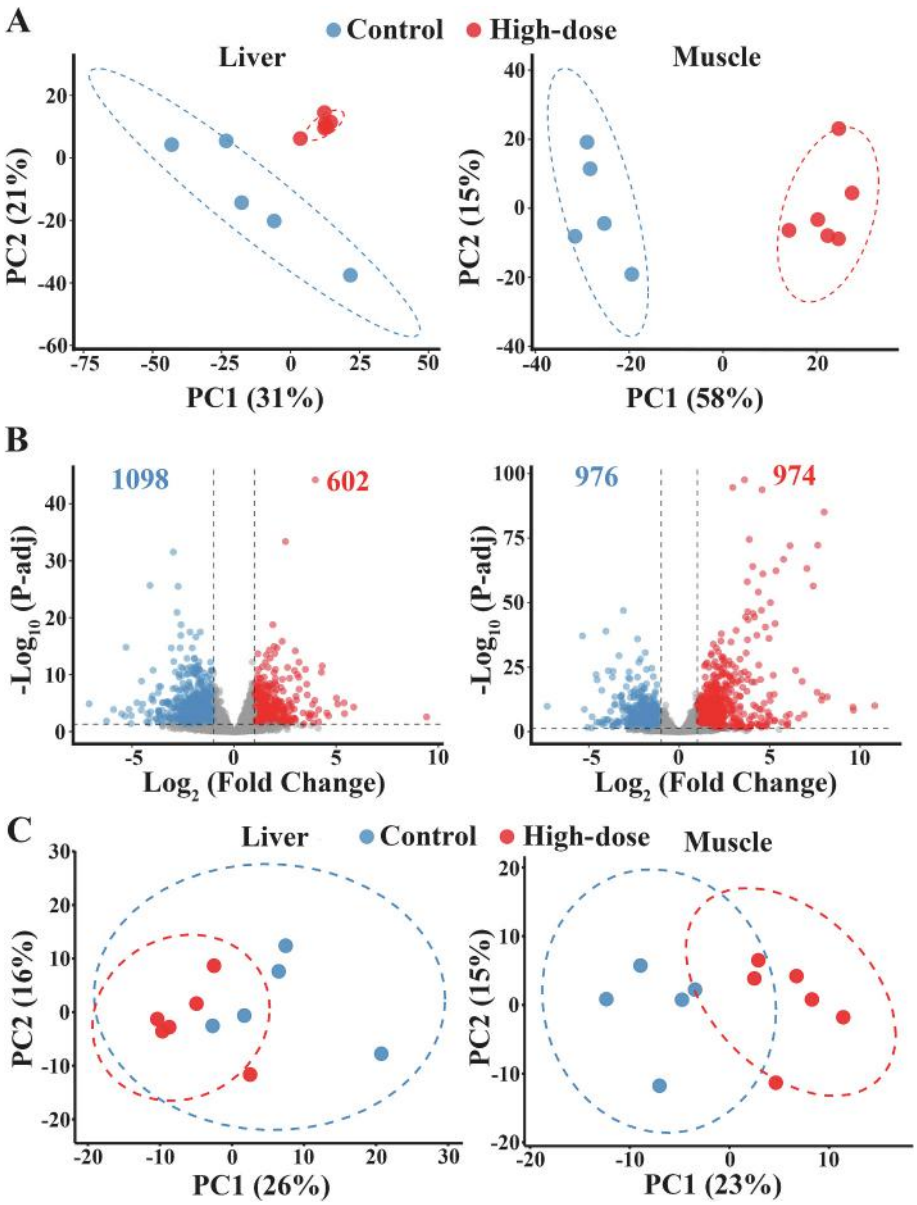


Fig. 3. Tissue-specific transcriptomic divergence and functional dissociation of the growth axis.
(A) PCA plots illustrating global transcriptomic profiles in liver (left) and muscle (right) tissues. (B) Volcano plots showing differentially expressed genes (DEGs) in the liver and muscle. Red and blue dots represent upregulated and downregulated genes, respectively. (C) PCA plots of metabolomic profiles for liver (left) and muscle (right). (For interpretation of the references to colour in this figure legend, the reader is referred to the web version of this article.)

and Table S6). This receptor-level upregulation was accompanied by markedly increased expression of downstream contractile proteins, notably the myosin heavy chain gene *myh7*, which exhibited up to a 50-fold induction in high-growth individuals (Fig. 4B and Table S6).

To characterize the metabolic substrates supporting this rapid protein accretion, metabolomic analysis revealed a 20.8-fold surge in intramuscular nicotinamide levels (Fig. 4C), which was highly synchronized with the upregulation of *nampt*, the rate-limiting enzyme of the NAD+ salvage pathway. Paradoxically, the intensified metabolic activity in muscle led to a significant downregulation of the local circadian regulator *clock* (Fig. 4E and Table S6), coinciding with reduced expression of the local circadian regulator clock.

3.5. Hepatic stress-associated transcriptional and metabolic changes

The liver exhibited pronounced stress-associated transcriptional changes and marked alterations in metabolic profiles under high-dose Rg5 treatment. The endoplasmic reticulum (ER) stress chaperone *hspa5* was induced up to 30-fold (Fig. 4F and Table S6), indicating an pronounced protein secretory burden. To maintain energy supply, the liver upregulated the gluconeogenic enzyme *g6pc* (Fig. 4G and Table S6) at the cost of its anabolic reserves, evidenced by the marked reduction of hepatic 3-HP (Fig. 4H). These quantitative signatures indicate coordinated changes in hepatic stress markers and metabolic pathways accompanying enhanced peripheral growth.

3.6. Associations between growth-, metabolism-, and stress-related indicators

Correlation analysis further substantiated the homeostatic decoupling. Muscular *igf1r* expression positively correlated with the WGR (Fig. 5A), showing a positive association with growth performance. Muscular *nampt* expression was highly synchronized with the burst in nicotinamide (Fig. 5B), supporting the altered metabolic allocation

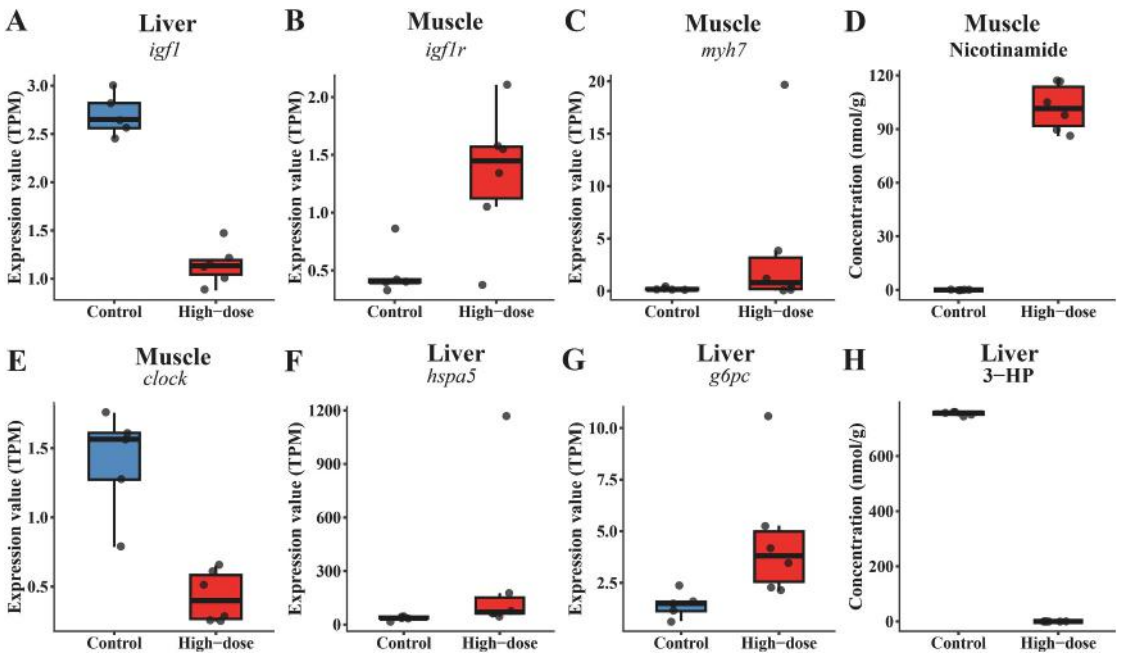


Fig. 4. Tissue-specific transcriptional and metabolic responses to high-dose Rg5.
(A) Hepatic *igf1* mRNA expression following Rg5 treatment. (B) Muscular *igf1r* expression levels. (C) Muscular *myh7* expression levels. (D) Nicotinamide concentrations in muscle tissue. (E) Muscular *clock* expression levels. (F) Hepatic *hspa5* expression levels. (G) Hepatic *g6pc* expression levels (Table S6). (H) Hepatic 3-hydroxypropionic acid (3-HP) concentrations. Data are presented as mean ± SEM. Statistical significance was assessed using a two-tailed *t*-test. Muscle (B–E), liver (A, F—H). Data represent normalized expression levels (TPM) obtained from RNA-Seq analysis.

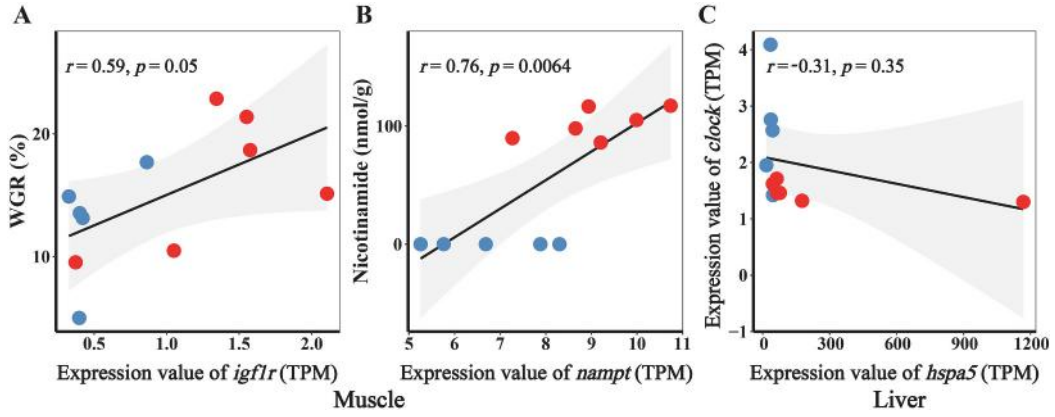


Fig. 5. Correlation analysis of growth-, metabolism-, and stress-related indicators.
(A) Correlation between muscular *igf1r* expression and weight gain rate (WGR). (B) Correlation between muscular *nampt* expression and nicotinamide levels. (C) Correlation between hepatic *hspa5* and *clock* expression levels. Pearson correlation coefficients (*r*) and corresponding *p*-values are shown. Shaded areas represent 95% confidence intervals.

pattern. Conversely, in the liver, the increased stress load (*hspa5*) displayed an inverse relationship trend with the circadian regulator *clock* (Fig. 5C and Table S6). These findings suggest that the metabolic prioritization of peripheral muscle growth occurs at the expense of hepatic homeostatic stability, accompanied by altered expression patterns of growth- and circadian-related genes.

4. Discussion

In aquaculture, enhancing somatic growth through nutritional or pharmacological interventions requires consideration of systemic physiological responses beyond the target tissue. Using an integrated multi-omics approach, this study characterized tissue-specific transcriptional and metabolic changes associated with high-dose ginsenoside Rg5 treatment in grass carp. While a clear increase in muscle mass and growth performance was observed, the accompanying molecular profiles indicate coordinated alterations across muscle and liver tissues.

Vertebrate somatic growth is classically regulated by the GH–IGF axis, in which hepatic IGF1 acts as a central endocrine mediator (Malespin and Nassri, 2019; Werner, 2023). In this context, the observed reduction in hepatic *igf1* expression alongside pronounced muscle hypertrophy appears counterintuitive. However, similar dissociations between hepatic *IGF1* production and peripheral growth responses have been reported under conditions of exogenous growth factor stimulation or receptor-level activation (Courtland et al., 2011; List et al., 2014; Cho et al., 2015; Kim et al., 2023). Our data suggest that, under high-dose Rg5 exposure, local enhancement of muscular *igf1r* expression may partially compensate for reduced hepatic *igf1* transcription, allowing somatic growth to proceed in a manner that is less dependent on canonical endocrine signaling. Rather than contradicting the GH–IGF

model, these findings suggest its plasticity under pharmacological perturbation.

Beyond growth signaling, our results point to pronounced metabolic adjustments accompanying muscle hypertrophy. The substantial increase in intramuscular nicotinamide levels, together with elevated nampt expression, is consistent with enhanced NAD^+ salvage activity, a pathway known to support high rates of protein synthesis and cellular growth (Garten et al., 2015). At the same time, the marked depletion of hepatic 3-hydroxypropionic acid suggests altered hepatic carbon flux. As 3-HP occupies a central position linking carbohydrate and lipid metabolism (Liang et al., 2022), its reduction may reflect a shift in hepatic metabolic priorities under sustained peripheral demand. Such tissue-level reallocation of metabolic substrates aligns with broader theoretical frameworks describing growth as a process constrained by energy and resource trade-offs (Huber, 2018; Rosenfeld et al., 2020; Robert Burger et al., 2021).

The induction of hepatic *hspa5* further indicates activation of stress-related pathways under high-dose Rg5 treatment. Elevated ER stress responses are commonly observed in metabolically active tissues experiencing increased protein folding and secretory demands (Ariyasu et al., 2017). In parallel, altered expression levels of circadian regulators (*clock* and *arntl*) was detected at the specific sampling window in both liver and muscle tissues. Although this study did not directly assess circadian rhythmicity over a 24-h cycle, accumulating evidence suggests that ER stress and unfolded protein responses can interfere with circadian gene expression, particularly under conditions of sustained metabolic challenge (Yuan et al., 2017; Gao et al., 2019; Dijk and Duffy, 2020; Koronowski and Sassone-Corsi, 2021; Ong and Logue, 2023). Within this framework, the observed changes in circadian gene expression may represent a secondary consequence of prolonged metabolic and proteostatic stress rather than a primary effect of Rg5 itself. Importantly, as samples were collected at a single time point, we cannot distinguish between a total suppression of rhythmicity and a phase shift in gene expression; hence, these results should be interpreted as localized transcriptomic alterations during the sampling window.

From an applied perspective, these findings underscore that pharmacological growth promotion can elicit complex systemic responses that extend beyond the target tissue. While high-dose Rg5 effectively enhances muscle growth, the accompanying metabolic and stress-related changes in the liver raise questions regarding long-term physiological sustainability. Importantly, while intraperitoneal injection provides a precise pharmacological model to identify these pathways, its direct application in large-scale aquaculture is limited. Our observations of hepatic stress suggest that future research should focus on developing oral administration or slow-release feeding strategies. Such controlled delivery methods could potentially maintain steady peripheral growth signaling while mitigating the acute metabolic burden and stress responses observed with bolus administration. Consequently, future studies incorporating time-series sampling, circadian functional assays, and extended exposure periods will be essential to clarify whether these responses represent transient adaptations or persistent constraints. Such insights will be critical for optimizing growth-promoting strategies that balance production efficiency with organismal health in sustainable aquaculture systems.

5. Conclusion

In summary, high-dose Ginsenoside Rg5 drives somatic growth in grass carp not by enhancing the endogenous axis, but by shifting its regulatory mode. The drug acts as a peripheral accelerator for muscle hypertrophy while forcing the liver into a stress-responsive, gluconeogenic survival mode. Furthermore, this physiological trade-off is associated with ER stress and altered expression of core clock genes within the specific sampling window. This study elucidates the hidden metabolic costs of pharmacological growth promotion and suggests that monitoring hepatic health markers is essential for the sustainable application of such growth enhancers in aquaculture.

CRediT authorship contribution statement

Li Ren: Supervision, Project administration, Methodology, Investigation, Funding acquisition, Data curation, Conceptualization. **Xiaohuan Han:** Investigation. **Qingxi Wang:** Validation. **Kai Yang:** Investigation. **Jinhui Zhang:** Investigation. **Ruyi Zhang:** Investigation. **Yude Wang:** Resources. **Yiyan Zeng:** Investigation. **Ling Liu:** Investigation. **Wei Liu:** Validation. **Wuhui Li:** Supervision, Resources, Conceptualization. **Shaojun Liu:** Methodology, Funding acquisition, Conceptualization.

Ethics approval and consent to participate

All experimental procedures involving animals were reviewed and approved by the Animal Ethics Committee of Hunan Normal University, Hunan, China (No. 2025003).

Declaration of competing interest

The authors declare that they have no known competing financial interests or personal relationships that could have appeared to influence the work reported in this paper.

Acknowledgements

This research was supported by National Key Research and Development Program of China (2023YFD2401602), National Natural Science Foundation of China (32341057 and 32293252), Special Funds for Construction of Innovative Provinces in Hunan Province (2021NK1010), Earmarked Fund for Agriculture Research System of China (CARS-45), and 111 Project (D20007), and The world-class cultivation discipline (Biology) of Hunan province.

Appendix A. Supplementary data

Supplementary data to this article can be found online at https://doi.org/10.1016/j.cbd.2026.101798.

Data availability

All raw sequencing data generated in this study (Whole-genome sequencing and Transcriptome) have been deposited in the Genome Sequence Archive (GSA) of the China National Center for Bioinformation under accession numbers CRA036829 and CRA036895, respectively. All data are publicly accessible at (https://ngdc.cncb.ac.cn/gsa).

References

Ariyasu, D., Yoshida, H., Hasegawa, Y., 2017. Endoplasmic reticulum (ER) stress and endocrine disorders. Int. J. Mol. Sci. 18.

Bouhaddani, S.E., Uh, H.W., Jongbloed, G., Hayward, C., Klarić, L., Kiełbasa, S.M., Houwing-Duistermaat, J., 2018. Integrating omics datasets with the OmicsPLS package. BMC bioinformatics 19, 371.

Chakraborty, S.B., Horn, P., Hancz, C., 2014. Application of phytochemicals as growth-promoters and endocrine modulators in fish culture. Rev. Aquac. 6, 1–19.

Chakravarthy, M.V., Siddiqui, M.S., Forsgren, M.F., Sanyal, A.J., 2020. Harnessing Muscle-Liver Crosstalk to Treat Nonalcoholic Steatohepatitis. Front. Endocrinol. 11, 592373.

Chen, S., Zhou, Y., Chen, Y., Gu, J., 2018. fastp: an ultra-fast all-in-one FASTQ preprocessor. Bioinformatics 34, i884–i890.

Cho, Y.L., Hur, S.M., Kim, J.Y., Kim, J.H., Lee, D.K., Choe, J., Won, M.H., Ha, K.S., Jeoung, D., Han, S., Ryoo, S., Lee, H., Min, J.K., Kwon, Y.G., Kim, D.H., Kim, Y.M., 2015. Specific activation of insulin-like growth factor-1 receptor by ginsenoside Rg5 promotes angiogenesis and vasorelaxation. J. Biol. Chem. 290, 467–477.

Cingolani, P., Platts, A., Wang le, L., Coon, M., Nguyen, T., Wang, L., Land, S.J., Lu, X., Ruden, D.M., 2012. A program for annotating and predicting the effects of single

nucleotide polymorphisms, SnpEff: SNPs in the genome of Drosophila melanogaster strain w1118; iso-2; iso-3. Fly 6, 80–92.
Courtland, H.W., Sun, H., Beth-On, M., Wu, Y., Elis, S., Rosen, C.J., Yakar, S., 2011. Growth hormone mediates pubertal skeletal development independent of hepatic IGF-1 production. J. Bone Miner. Res. 26, 761–768.
Danecek, P., Auton, A., Abecasis, G., Albers, C.A., Banks, E., DePristo, M.A., Handsaker, R.E., Lunter, G., Marth, G.T., Sherry, S.T., McVean, G., Durbin, R., Genomes Project Analysis, G, 2011. The variant call format and VCFtools. Bioinformatics 27, 2156–2158.
Dijk, D.J., Duffy, J.F., 2020. Novel Approaches for Assessing Circadian Rhythmicity in Humans: A Review. J. Biol. Rhythm. 35, 421–438.
Gao, L., Chen, H., Li, C., Xiao, Y., Yang, D., Zhang, M., Zhou, D., Liu, W., Wang, A., Jin, Y., 2019. ER stress activation impairs the expression of circadian clock and clock-controlled genes in NIH3T3 cells via an ATF4-dependent mechanism. Cell. Signal. 57, 89–101.
Garten, A., Schuster, S., Penke, M., Gorski, T., De Giorgis, T., Kiess, W., 2015. Physiological and pathophysiological roles of NAMPT and NAD metabolism. Nat. Rev. Endocrinol. 11, 535–546.
Hu, F., Zhong, H., Wu, C., Wang, S., Guo, Z., Tao, M., Zhang, C., Gong, D., Gao, X., Tang, C., Wei, Z., Wen, M., Liu, S., 2021. Development of fisheries in China. Reproduction and Breeding 1, 64–79.
Huber, K., 2018. Invited review: resource allocation mismatch as pathway to disproportionate growth in farm animals–prerequisite for a disturbed health. Animal: an international journal of animal bioscience 12, 528–536.
Karasov, T.L., Chae, E., Herman, J.J., Bergelson, J., 2017. Mechanisms to Mitigate the Trade-Off between Growth and Defense. Plant Cell 29, 666–680.
Kim, D., Paggi, J.M., Park, C., Bennett, C., Salzberg, S.L., 2019. Graph-based genome alignment and genotyping with HISAT2 and HISAT-genotype. Nat. Biotechnol. 37, 907–915.
Kim, D., Hwang, C.Y., Cho, K.H., 2024. The fitness trade-off between growth and stress resistance determines the phenotypic landscape. BMC Biol. 22, 62.
Kim, R., Kim, J.W., Choi, H., Oh, J.E., Kim, T.H., Go, G.Y., Lee, S.J., Bae, G.U., 2023. Ginsenoside Rg5 promotes muscle regeneration via p38MAPK and Akt/mTOR signaling. J. Ginseng Res. 47, 726–734.
Koronowski, K.B., Sassone-Corsi, P., 2021. Communicating clocks shape circadian homeostasis. Science 371, eabd0951.
Li, H., Durbin, R., 2010. Fast and accurate long-read alignment with Burrows-Wheeler transform. Bioinformatics 26, 589–595.
Li, H., Handsaker, B., Wysoker, A., Fennell, T., Ruan, J., Homer, N., Marth, G., Abecasis, G., Durbin, R., 2009. The sequence alignment/map format and SAMtools. Bioinformatics 25, 2078–2079.
Liang, B., Sun, G., Zhang, X., Nie, Q., Zhao, Y., Yang, J., 2022. Recent advances, challenges and metabolic engineering strategies in the biosynthesis of 3-hydroxy-propionic acid. Biotechnol. Bioeng. 119, 2639–2668.
Liao, Y., Smyth, G.K., Shi, W., 2014. featureCounts: an efficient general purpose program for assigning sequence reads to genomic features. Bioinformatics 30, 923–930.
List, E.O., Berryman, D.E., Funk, K., Jara, A., Kelder, B., Wang, F., Stout, M.B., Zhi, X., Sun, L., White, T.A., 2014. Liver-specific GH receptor gene-disrupted (LiGHRKO) mice have decreased endocrine IGF-I, increased local IGF-I, and altered body size, body composition, and adipokine profiles. Endocrinology 155, 1793–1805.
Love, M., Anders, S., Huber, W., 2014. Differential analysis of count data–the DESeq2 package. Genome Biol. 15, 10–1186.
Malespin, M., Nassri, A., 2019. Endocrine diseases and the liver: an update. Clin. Liver Dis. 23, 233–246.
Mckenna, A., Hanna, M., Banks, E., Sivachenko, A., Cibulskis, K., Kernytsky, A., Garimella, K., Altshuler, D., Gabriel, S., Daly, M., 2010. The Genome Analysis Toolkit: A MapReduce framework for analyzing next-generation DNA sequencing data. Genome Res. 20, 1297–1303.
Ong, G., Logue, S.E., 2023. Unfolding the interactions between endoplasmic reticulum stress and oxidative stress. Antioxidants 12, 981.
Robert Burger, J., Hou, C., AS Hall, C., Brown, J.H., 2021. Universal rules of life: metabolic rates, biological times and the equal fitness paradigm. Ecol. Lett. 24, 1262–1281.
Rosenfeld, J., Richards, J., Allen, D., Van Leeuwen, T., Monnet, G., 2020. Adaptive trade-offs in fish energetics and physiology: insights from adaptive differentiation among juvenile salmonids. Can. J. Fish. Aquat. Sci. 77, 1243–1255.
Wang, Y., Liu, W., Li, Z., Qiu, B., Li, J., Geng, G., Hu, B., Liao, A., Cai, Y., Wen, M., Wang, S., Qin, Q., Luo, K., Liu, S., 2024. Improvement and application of genetic resources of grass carp (Ctenopharyngodon idella). Reproduction and Breeding 4, 126–133.
Werner, H., 2023. The IGF1 signaling pathway: from basic concepts to therapeutic opportunities. Int. J. Mol. Sci. 24, 14882.
Yu, G., Wang, L.G., Han, Y., He, Q.Y., 2012. clusterProfiler: an R package for comparing biological themes among gene clusters. Omics: a journal of integrative biology 16, 284–287.
Yuan, G., Hua, B., Cai, T., Xu, L., Li, E., Huang, Y., Sun, N., Yan, Z., Lu, C., Qian, R., 2017. Clock mediates liver senescence by controlling ER stress. Aging 9, 2647.
Zhang, X.Y., Khakisahneh, S., Han, S.Y., Song, E.J., Nam, Y.D., Kim, H., 2024. Ginseng extracts improve circadian clock gene expression and reduce inflammation directly and indirectly through gut microbiota and PI3K signaling pathway. NPJ Biofilms Microbiomes 10, 24.